Indian Journal of Chemistry
Vol. 64, February 2025, pp. 127-136
DOI: 10.56042/ijc.v64i2.9761

Chitosan augmented activated charcoal for adsorption of reactive red 21 dye from solution phase

P M Nandanwar* & R M Jugade

Department of Chemistry, RTM Nagpur University, Nagpur 440 033, India

E-mail: pradipnandanwar27@gmail.com, ravinj2001@yahoo.co.in

Received 20 March 2024; accepted (revised) 22 January 2025

Polymers have been proven to be an interesting class of adsorbents applied in water treatment. Biopolymers are of special interest due to their unique properties such as biocompatibility, biodegradability and reusability. This work reports a composite formed by a chitosan biopolymer and activated charcoal using sodium citrate as a crosslinking agent. The chitosan–citrate-activated charcoal composite (CCA) has been characterized using FT–IR, SEM, EDAX, XRD, TGA–DTA and BET surface area analysis. The material has been found to be microporous in nature with a surface area of 165.83 m^2/g that has led to high adsorption capacities toward the targeted pollutant. In aqueous phase, the dye adsorption studies have been carried out with reactive 21 (R-21) dye. Under optimum solution conditions, maximum Reactive Red (R-21) dye removal capacity has been found to be 40.12 mg g^{-1}. Intrinsic microporosity of CCA results in an enhanced capture capacity for Reactive Red (R-21) dye. Material sustainability studies have been carried out to evaluate various sustainability parameters.

Keywords: Adsorption, Isotherm, R-21, Thermodynamics

Natural polymers based on plant and non-plants sources have been in focus as adsorbents for the majority of contaminants in order to provide a clean and safe environment. Natural polymers cleanse wastewater for its sustainable recirculation into the environment due to their inherent structure, composition, and diverse functionality along with important characteristic properties such as non-toxicity, low-cost, renewability, biodegradability, and biocompatibility[1]. A variety of natural polymers such as starch[2], pectin[3], chitin, chitosan[4], bacteria, algae, fungi[5], and ghatti gum[6] have been employed for decontamination of water. Nonetheless, in many cases, natural polymers are not sufficient to remove the dyes from highly complex dye-containing wastewater, and so these polymers should be subjected to a modification process, involving chemical or physical treatment, in order to enhance their efficiency in removing dyes from complex wastewater[7]. Composites of biopolymers have dominant properties such as improved durability, processing capability, high functionality, and a large surface area, which increase the removal of contaminants or pollutants from the environment *via* adsorption[8]. Recently, composites of natural polymers have come into focus as adsorbents for the majority of contaminants. These natural polymers include cellulose[9], chitosan[10], sodium alginate[11], and other natural products[12] due to their abundance, non-toxicity, biodegradability, low cost, *etc*.

Chitosan is widely used as an adsorbent for contaminant removal in wastewater due to its distinct advantages of non-toxicity, cost-effectiveness, biodegradability, and super-high adsorption capacity[13]. However, due to its high solubility and swelling index in acidic media, and low surface area and mechanical strength, chitosan, on its own, is not a successful material for water treatment technology. Therefore, chemical modification through composition and/or a crosslinking process is an alternative way to increase mechanical resistance, reduce hydrophobicity and stabilize chitosan in acidic environments. A lot of research has been conducted on dye adsorption using chitosan in its native form[10] and on chitosan combinations such as chitosan/carbon composites[14], chitosan–vanadate films[15], cellulose/chitosan composites[16], surface-modified chitosan[17], chitosan-based cryogels[18], and β-cyclodextrin–chitosan-based cross-linked adsorbents[19]. Blending of chitosan with other organic moieties and introducing magnetic properties to the composites have resulted in high selectivity and adsorption

efficiency towards target pollutants[20]. Advanced applications of natural-fiber-reinforced chitosan, chitosan blends and their nanocomposites have also been reviewed in the recent literature[21].

Our research group has reported various chitosan- and cellulose-based materials for the removal of organic dyes from water bodies. These include a chitosan–alginate composite[22], a tetrabutyl ammonium impregnated chitosan[23], a chitosan–bentonite composite[24], a chitosan–Mohr's salt composite[25], and a cellulose–tin composite[26]. Furthermore, recently, we have reported Chitosan entrapped microporous activated carbon composite as a supersorbent for remazol brilliant blue R (Ref. 27) and Chitosan-Biopolymer-Entrapped Activated Charcoal for Adsorption of Reactive Orange Dye from Aqueous Phase and CO_2 from Gaseous Phase[28]. The aim of this work is to synthesize an environmentally benign material that can be used as a water-treatment agent without using any drastic conditions and chemicals. To the best of our knowledge, this work is the first ever attempt to derive a material at room temperature that has all the following merits: the adsorption properties of charcoal, the biocompatibility of chitosan, and mechanical stability provided by a citrate crosslinker. Reactive Red (R-21) has been selected as a representative dye for this work. Such a material can be a boon to environmental scientists for multi-toxicant decontamination.

Materials and Methods

All the chemicals and reagents used were of analytical grade. Chitosan with a degree of deacetylation of >90% was purchased from Sisco Research Laboratory, Mumbai, India. Acetic acid and 25% ammonia solution were obtained from SD Fine Chemicals Ltd., Mumbai, India. Activated charcoal, sodium citrate, and reactive Red 21 dye were acquired from Loba Chemie, Mumbai, India. All chemicals were used without further purification and deionized distilled water was used throughout the studies. Chitosan solution was prepared by dissolving 5 g chitosan in 500 mL of 2% acetic acid with stirring for 60 min. After the complete dissolution of chitosan in acetic acid, 2.5 g activated charcoal was added in small instalments and the solution was kept on gentle stirring for 30 min. The resultant solution was dripped into a beaker containing 1000 mL of 6% ammonia solution with the help of a syringe, leading to the formation of spherical beads. The fresh beads were rinsed with distilled water several times for removal of all traces of ammonia. The beads were suspended in 250 mL of 1% sodium citrate solution and stirred slowly at 40°C for 2 h for the crosslinking process. The resulting CCA beads were washed with distilled water several times and dried overnight in a hot air oven at 50°C. The beads were crushed using a pestle and mortar and sieved with a 100 micron mesh before being used in the adsorption experiments. In each experiment, 25 mL dye solution of a pre-decided concentration along with a known weight of CCA, was stirred on a magnetic stirrer for a pre-determined time. It was then filtered and the residual R-21 dye concentration was evaluated spectrophotometrically at 521 nm using a Shimadzu 1900 UV-visible spectrophotometer (Shimadzu, Kyoto, Japan) with matched quartz cuvettes. Triplicate observations were obtained and the mean values are reported. The equilibrium adsorption efficiency in mg g^{-1} can be calculated using following equation[29].

$$q_e = \frac{C_0 - C_e}{W} \times V$$

where C_0 and Ce are the initial and equilibrium concentration of R-21 in solution in mg L^{-1}, respectively, V is the solution volume in L, and W is the weight of CCA used in g. Trial runs were performed to compare the adsorption efficiencies of unmodified and sequentially modified adsorbents for the reactive red 21 dye. For this, 50 mg L^{-1} dye solution was equilibrated for 60 min with 100 mg of unmodified chitosan, activated charcoal, sodium citrate crosslinked chitosan, and CCA composite in different flasks. The solution phase concentrations in each flask were determined after filtration and the adsorption efficiency was calculated for each of them. To study the effect of temperature as part of the evaluation of the thermodynamic parameters, the temperature was varied from 298 to 333 K. The quantity of adsorption of R-21 on CCA was investigated at an R-21 concentration of 100 mg L^{-1} using a 25 mL volume and adsorbent dose of 100 mg. In all the experiments, the original solutions as well as the treated solutions were filtered through Whatman no. 1 filter papers to overcome the effect of adsorption by filter paper. X-ray diffraction (XRD) spectra were recorded on an Ultima IV diffractometer (Cu Ka radiation, 40 kV and 20 mA) from $2\theta = 2°$ to 10° with a step size of 0.02° (Rigaku, Tokyo, Japan).

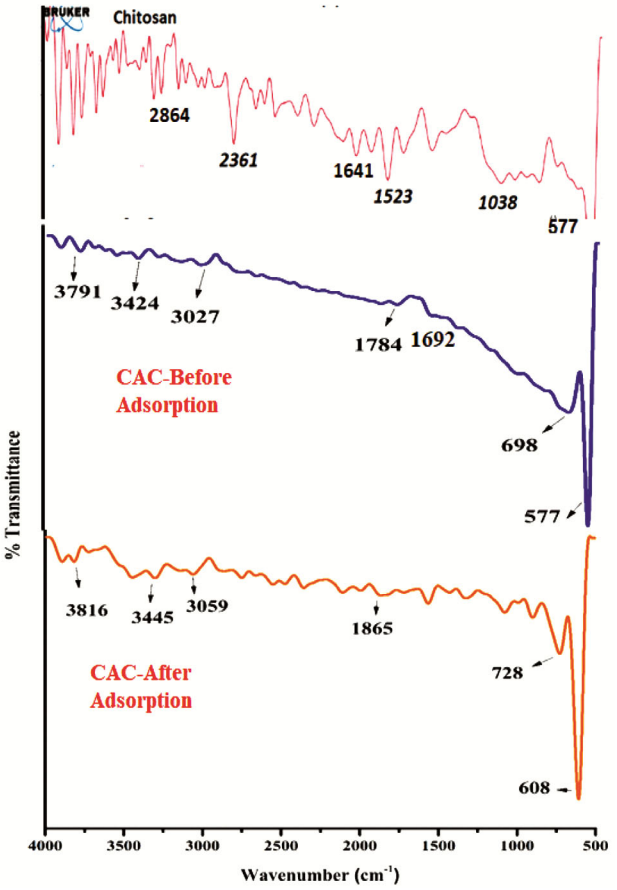

Fig. 1 — FTIR spectra of (a) chitosan and (b) CCA before adsorption (c) After Adsorption

The thermal stability of the synthesized material (CCA) was assessed in a DTG-60 simultaneous DTA/TG instrument (Shimadzu, Tokyo, Japan) in nitrogen medium. About 15 mg of the sample was loaded on a platinum pan with a heating rate of 20°C min−1 up to 900°C under 100 mL min−1 of flowing N_2. Fourier transform infrared (FTIR) spectra were obtained on a BrukerAlphaE, London, UK, spectrometer in the range 500–4000 cm^{-1} using KBr pellets. The textural properties of the adsorbent were assessed using a scanning electron microscope (SEM) model TESCAN VEGA 3 SBH. Energy dispersive spectroscopy (EDAX) analysis was performed for elemental composition using an X-ray analyzer Oxford INCA Energy 250 EDS system during SEM observations. The samples were degassed at 150°C for 2 h under vacuum and N_2 adsorption/desorption isotherms were acquired samples were degassed at 150°C for 2 h under vacuum and N_2 adsorption/ desorption isotherms were acquired at −196°C on a Quantachrome Nova 2200e analyzer (Anton Paar, Graz, Austria). The surface area was calculated by considering the BET model, and the pore volume was obtained using the BJH method. The pH_{PZC} measurement was performed using an Equiptronics EQ-615 *p*H meter, the absorbance of the dyes was recorded using an Equiptronics EQ-824, while an Equiptronics magnetic stirrer model EQ-770 was used for batch adsorption stirring (Equiptronics, Mumbai, India). Linear regression analysis was used to determine the parameters of isotherms and kinetic models. Additionally, error analysis was carried out to ascertain the desired accuracy has been achieved.

$$SSE \text{ (error sum of squares)} = \Sigma (q_{e/t}{}^{exp} - q_{e/t}{}^{cal})^2$$

Where $q_{e/t}{}^{exp}$ and $q_{e/t}{}^{cal}$ are the experimental adsorption capacity at equilibrium or at any time ($q_{e/t}{}^{exp}$) and the calculated adsorption capacity at equilibrium or at any time ($q_{e/t}{}^{cal}$) from the models respectively.

$$AIC \text{ (Akaike Information Criterion)} = N \text{ Ln } SSE/N + 2K$$

Where, N is the number of data points and K is the number of parameters[30].

Results and Discussion

Characterization of CCA

FT–IR spectra of native chitosan showed (Fig. 1a) its characteristic vibrational peaks at 1021 cm^{-1} (C–O–C stretching), 1641 cm^{-1} (N–H stretching), 2864 cm^{-1} (C–H stretching), and 577 cm^{-1} (C–H bending)[31]. When CCA was formed, these bands shifted to higher wavenumbers while the spectrum was found to be highly complex (Fig. 1b). In addition to that, the peak observed at 698 cm^{-1} is due the C–H bending and deformation frequencies of the cross-linker sodium citrate. The C=O stretching band was found to get intensified at 1692 cm^{-1}. This indicates cross-linking of sodium citrate with chitosan involving electrostatic interactions[32]. All the significant peaks shifted towards higher chemical shifts upon adsorption can be depicted in Fig. 1c.

Fig. 2 shows the X-ray diffractograms of chitosan and CCA. Native chitosan showed characteristic peaks at 2θ = 10.92° and 20.01° corresponding to (020) and (110) planes, respectively[33]. In case of CCA, these two peaks were found to shift towards lower values. The decrease in crystallinity of adsorbent can be attributed to the typical amorphous regions of chitosan which are established through intramolecular and intermolecular H-bonding

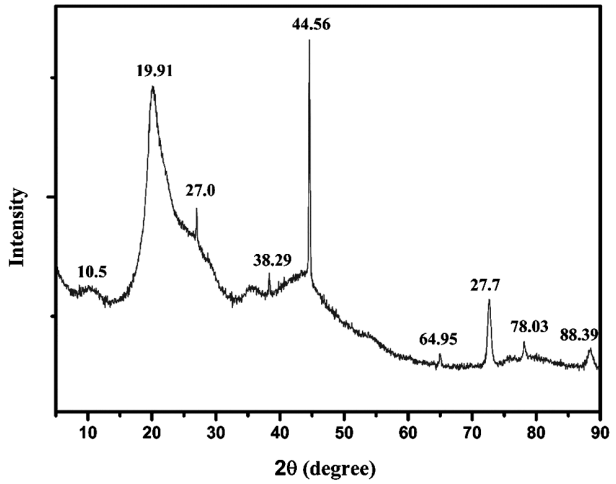

Fig. 2 — XRD patterns of CCA

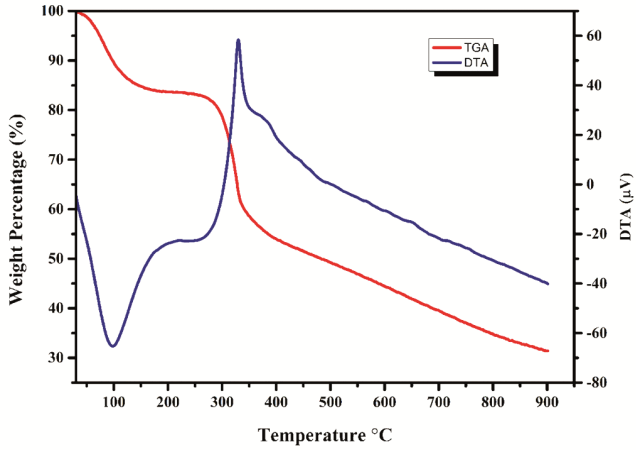

Fig. 3 — TGA and DTA curves of CCA

interactions. The XRD pattern of CCA shows additional peaks at 2θ = 44.56°, 72.7°, and 88.39° corresponding to various planes of sodium citrate[34].

Thermal analyses (Fig. 3) were performed to evaluate the stability of the adsorbent at elevated temperatures, as this property is important to ensure its further use during several temperature and pressure swings. The TGA curve of chitosan showed two sharp weight losses due to loss of moisture and adsorbed water up to 120°C and thermal decomposition between 275 and 325°C. The total weight loss was found to be almost 100%. The composite material CCA also exhibited two sharp weight loss events. The first started at ambient temperatures going up to approximately 150°C and is associated with the loss of physically adsorbed water. The second loss occurred in the range 325–400°C. This shows enhanced thermal stability in comparison to the native chitosan. A gradual decomposition occurred above 400°C corresponding to the complete decomposition of chitosan and the destruction of citrate crosslinking. The DTA curves presented endothermic peaks corresponding to moisture loss in both the materials and exothermic peaks for thermal decay. The shift in exotherm to higher temperature in CCA is a clear indication of formation of composite between chitosan and activated charcoal with the citrate crosslinker, as well as increased thermal stability of CCA.

N_2 adsorption/desorption isotherms of CCA as depicted in Fig. 4 showed the N_2 physisorption isotherm was type IV according to the IUPAC classification. This result indicated the presence of micropores in its structure. The pure chitosan was found to have a surface area of 0.013 $m^2\ g^{-1}$ with a pore volume of $1.263 \times 10^{-3}\ cm^3\ g^{-1}$ while those of activated charcoal were 897.9 $m^2\ g^{-1}$ and 12.29 $cm^3\ g^{-1}$. This indicates a non-porous nature of chitosan and a highly porous nature of activated charcoal. The surface area of CCA was 165.83 $m^2\ g^{-1}$ with a pore volume of 1.332 $cm^3\ g^{-1}$. The mean pore radius of CCA was found to be 1.459 nm, indicating that it is a microporous material[35]. The intermediate surface area of CCA is indicative of formation of composite and loading of chitosan into the porous framework of activated charcoal. The adsorption–desorption isotherm shows a small hysteresis loop of the H4 type. Such a loop is observed if the material is highly complex showing microporosity as well as mesoporosity. This observation is consistent with the granular-like appearance of the surface of the material as obtained in SEM micrographs. The isotherm shows that desorption curves shifted to lower values than adsorption curves, which can be attributed to cavitation-persuaded desertion[36]. The high adsorption capacity of CCA towards R-21 dye can be prominently attributed to the high surface area, large pore volume, and micro and mesoporous nature of the adsorbent.

The SEM micrographs show the surface morphology of the modified adsorbent (Fig. 5a). Chitosan has a relatively smooth and regular surface compared to CCA which has an irregular and heterogeneous surface. The porous and folded surface of the adsorbent enhances the surface area and therefore the adsorption capacity.

The EDAX (Fig. 5b) technique was used to analyze the elemental composition of CCA. CCA have elemental C, N, and O as constituent elements, along with a slight impurity of Na in CCA.

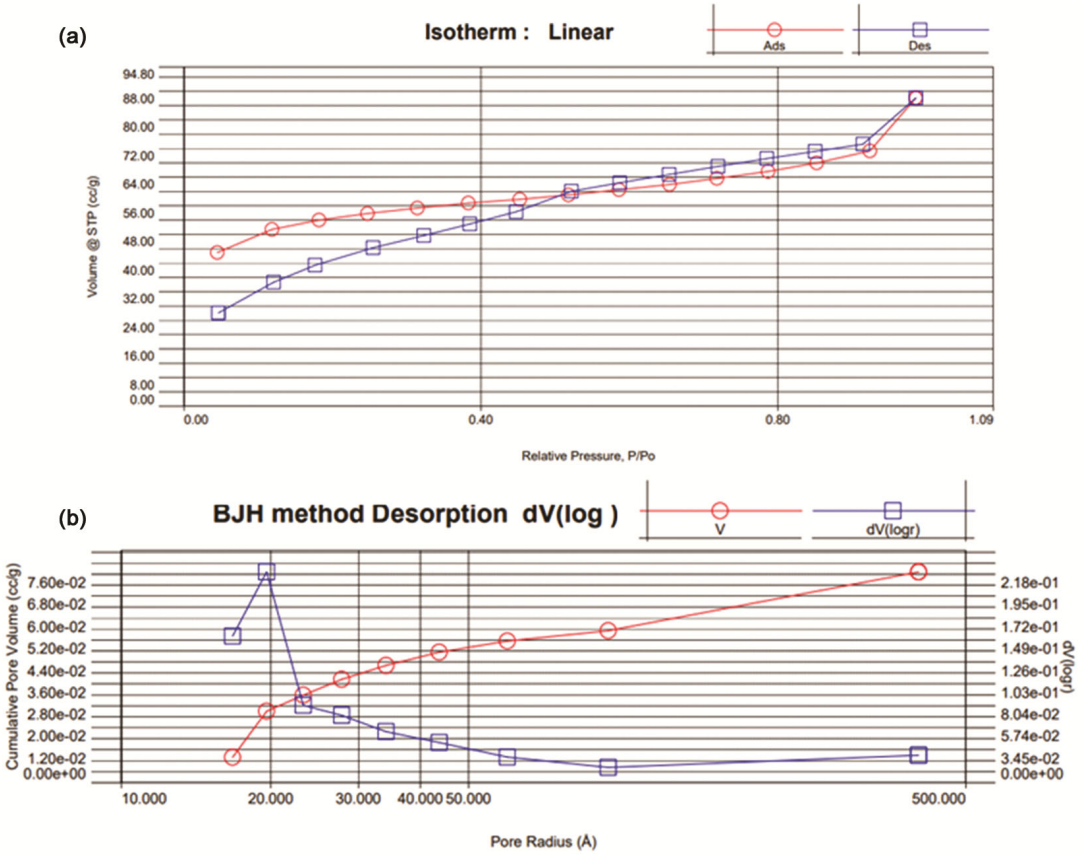

Fig. 4 — (a) N_2 adsorption–desorption isotherms, (b) pore size distribution of CCA

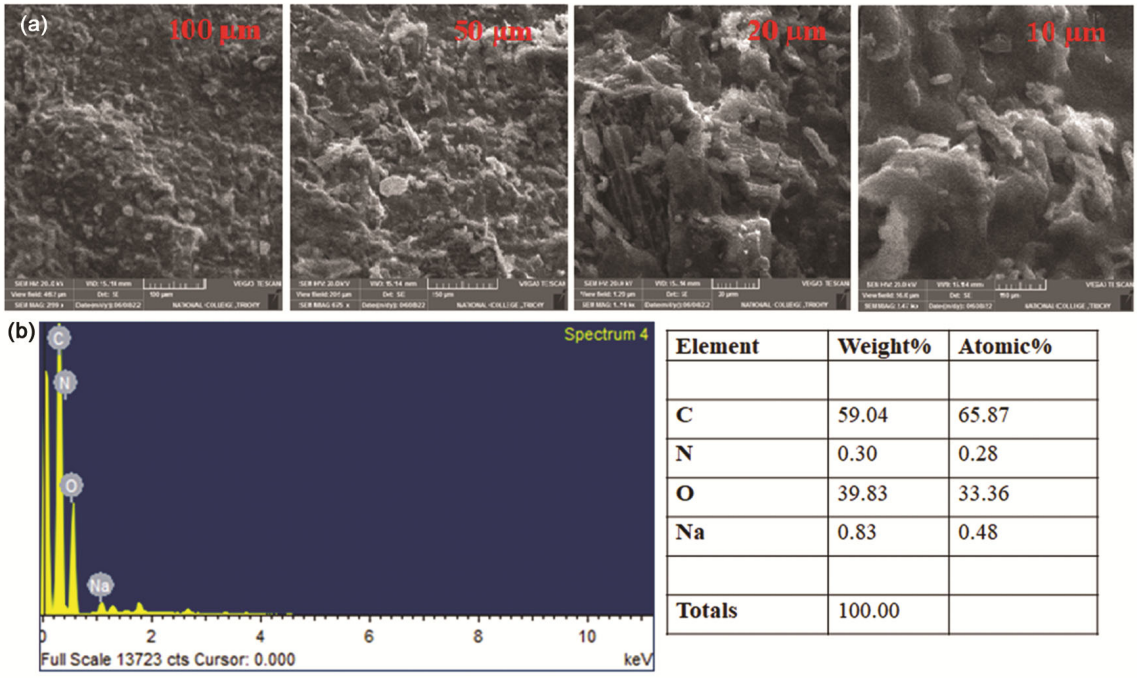

Element	Weight%	Atomic%
C	59.04	65.87
N	0.30	0.28
O	39.83	33.36
Na	0.83	0.48
Totals	100.00	

Fig. 5 — (a) SEM micrographs of CCA at different scale, (b) EDAX of CCA

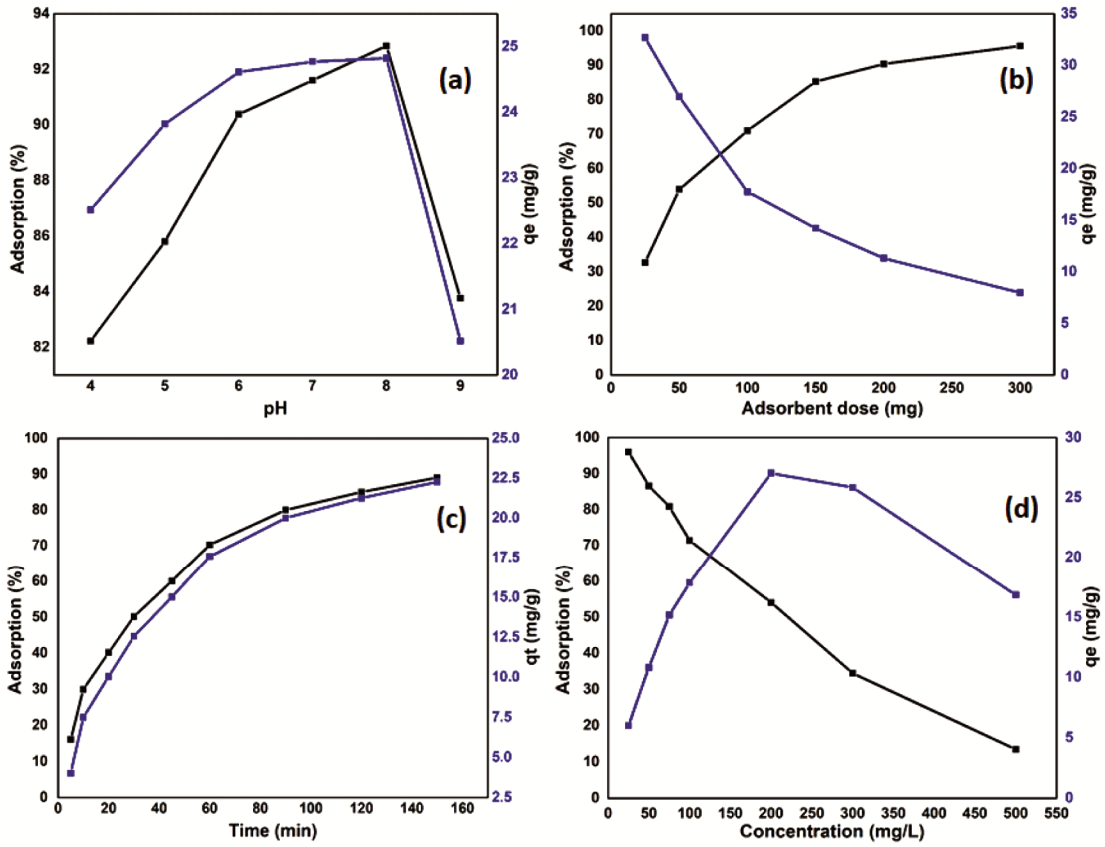

Fig. 6 — (a) Effect of *p*H, (b) effect of adsorbent dose, (c) effect of adsorption time, and (d) effect of concentration on adsorption of R-21 dye (Blak = Adsorption % and Blue = qe)

Optimization of Adsorption Equilibrium Parameters

The *p*H of the R-21 dye solution greatly influences the adsorption process, and thus the impact of solution *p*H on adsorption was studied. The *p*H of the R-21 dye varied from *p*H 4.0 to 8.0 and was equilibrated with a 100 mg CCA dose for 60 min on magnetic stirrer. Fig. 6a shows that the R-21 dye removal reached a maximum at *p*H 8. Under acidic conditions, the nitrogen atoms of both chitosan and R-21 dye get protonated, leading to repulsive interaction. Under stronger basic conditions, as the *p*H exceeds 8.2, the surface charge of CCA becomes negative and it repels the anionic dye molecules[37]. Hence, it is quite obvious that the electrostatic interaction is strongly attractive at a near-neutral *p*H between 7 and 8. Hence, *p*H 8.0 was maintained throughout the studies (Fig. 6a). At *p*H 9.0, the surface charge of material becomes negative, thereby repelling the anionic dye. This could be reflected in a sudden decrease in adsorption efficiency at *p*H 9.0.

In order to determine the effect of CCA dosage on the removal of R-21 dye, the dose was varied from 25 mg to 300 mg and equilibrated with 100 mg L^{-1} R-21 dye for 60 min. With an increase in the adsorbent dose, the rate of adsorption was found to increase due to availability of more and more adsorption sites. When the available dye molecules were completely adsorbed, a plateau was obtained at above 100 mg adsorbent. The adsorption efficiency in terms of qe (mg g^{-1}) was found to be high at lower adsorbent doses and further decreased with an increase in dose (Fig. 6b). Above 100 mg adsorbent dose the removal of R-21 dye is more than 70% and thus 100 mg dose was fixed for further studies.

In order to determine the effect of contact time, the time was varied from 5 to 150 min. From Fig. 6c, it can be seen that there is a rapid increase in adsorption up to 60 min, leading to saturation of adsorbent surface. Equilibrium was achieved, and so negligible variation was observed after this. Thus, 60 min time was fixed for further studies. A range of initial R-21 dye concentrations were used in the adsorption studies, ranging from 25 mg L^{-1} to 500 mg L^{-1}. The study was carried out at previously optimized parameters with a fixed dose, time, and original *p*H of dye solution. More than 70% adsorption was observed

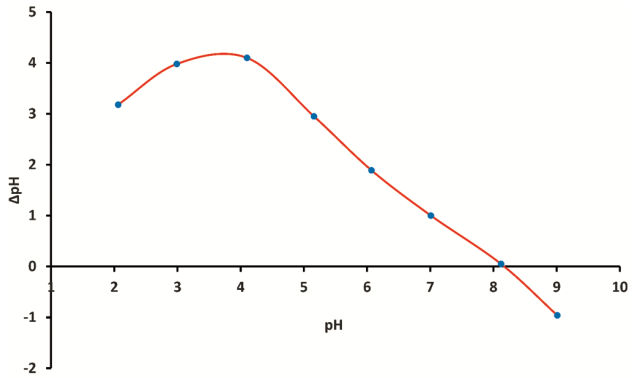

Fig. 7 — The pH_{PZC} of CCA

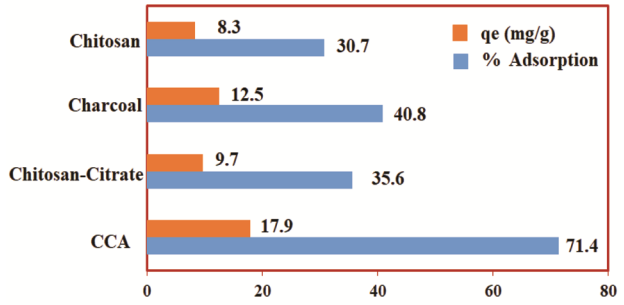

Fig. 8 — Comparison of various materials for removal of R-21 dye

up to 100 mg L^{-1}, then it decreased rapidly with further increase in dye concentration due to saturation of adsorbent surface (Fig. 6d). The efficiency of material was found to be maximum at an R-21 dye concentration of 300 mg L^{-1}. The surface charge on the adsorbent was evaluated using pH_{PZC}. It is the *p*H at which the charge on the adsorbent surface is zero. In order to determine pH_{PZC}, 50 mL of 0.1 M NaCl solutions which varied in *p*H from 2.0 to 9.0 were taken in separate conical flasks. 100 mg CCA was added to each system and the solutions were stirred for 24 h. The solutions were filtered, and the *p*H values of the filtrates were determined. From the plot of Δ*p*H *versus* initial *p*H, the pH_{PZC} of the adsorbent was determined to be 8.2 (Fig. 7). When the solution *p*H is less than 8.2, the charge on the adsorbent surface is positive and thus it will take up negative ions and when the charge on the adsorbent surface is negative it will take up positive ions[38].

Screening Runs

In order to check the applicability of CCA for R-21 dye confiscation, the four materials were selected. A total of 100 mg each of chitosan, activated charcoal, citrate-crosslinked chitosan, and CCA was added to 25 mL of 100 mg L^{-1} R-21 dye solution in separate conical flasks and stirred for 60 min. The solutions were filtered and residual concentrations of filtrates were evaluated. The adsorption capacities and percentage adsorption of the four materials are compared in Fig. 8. It was observed that all the four materials have a tendency to adsorb R-21 dye. However, the capacity was maximum for CCA with more than 90% adsorption. Hence, it can be concluded that CCA is an admirable adsorbent for R-21 dye.

Isotherm Study

Adsorption isotherm models such as Freundlich[39] and Langmuir[40] were studied, which gave a better understanding of the adsorption mechanism (Fig. 9a, b). The adsorption studies were carried by equilibrating 25 mL of R-21 dye solution by increasing the concentration from 25 to 500 mg L^{-1} with 100 mg adsorbent for 60 min. From Table 1 it can be seen that the correlation coefficient value is quite close to unity for the Langmuir isotherm. From the R^2 value it can be concluded that there is a monolayer formation of R-21 on CCA in accordance with the Langmuir model. The Freundlich isotherm shows the value of n is 0.779 which specifies a chemisorption process of adsorption. The adsorption capacity of R-21 dye is depicted in Table 1.

Kinetics of Adsorption

The measure of progress of R-21 dye adsorbed on the CCA depends on contact time and thus the kinetics of adsorption were studied using pseudo-first- and pseudo-second order reactions. Experiments were carried out at concentration of 100 mg L−1 by varying time from 5 to 150 min with 100 mg adsorbent. The plots of kinetics of adsorption for R-21 dye were studied and the results are depicted in Fig. 9c,d. The values of the correlation coefficients for both models were found to be close to 1 for pseudo-second-order kinetics, it can be concluded that it is best model to describe the R-21 dye adsorption on CCA, affirming chemisorption. The results are summarized in Table 1. Additionally, an intraparticle diffusion model designed by Weber and Morris[41] was used to identify if the adsorption process is controlled by diffusion only. Fig. 9e shows that the intercept between qt and $t_{1/2}$ is non-zero, indicating that

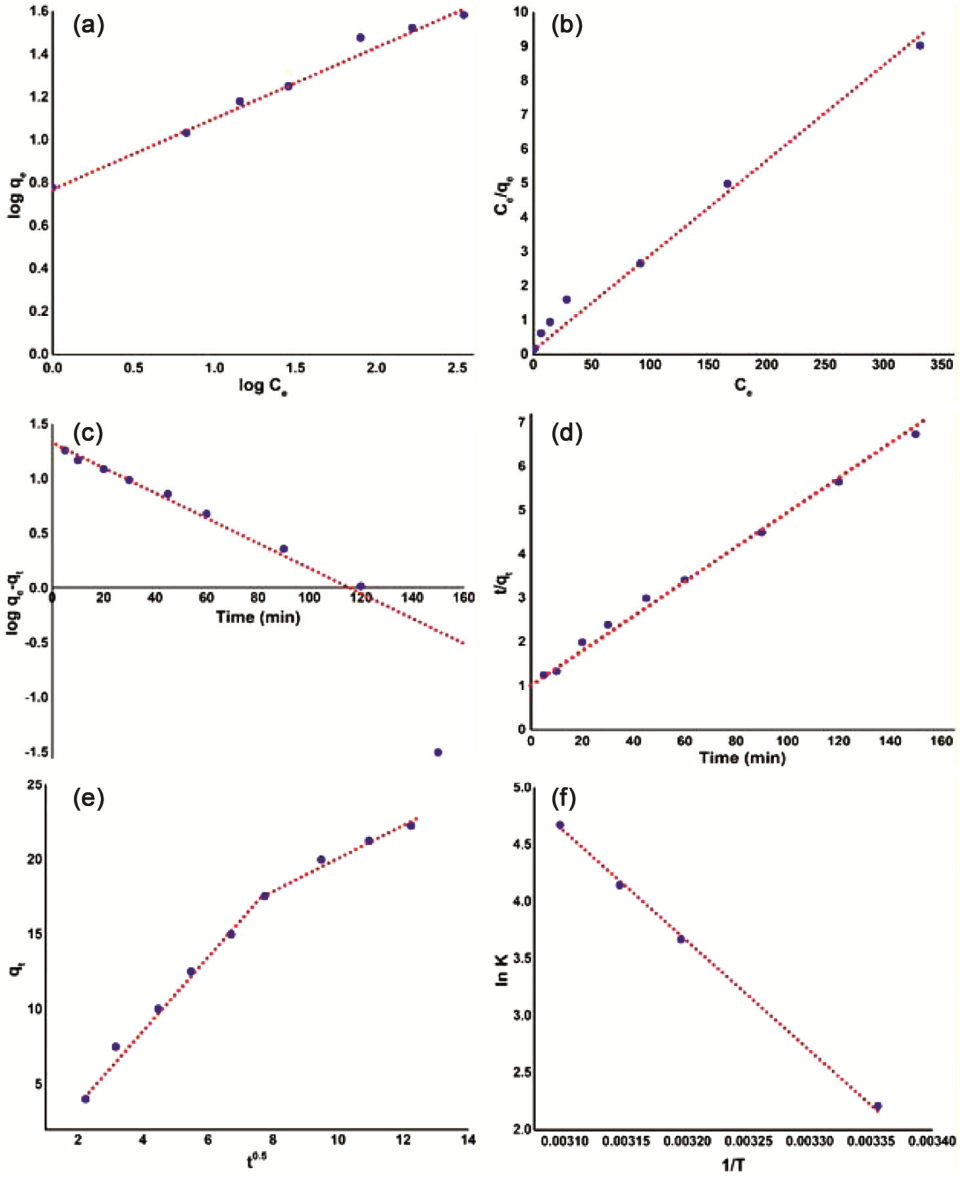

Fig. 9 — (a) Freundlich, (b) Langmuir, (c) Pseudo-first order, (d) Pseudo-second order (e) intraparticle diffusion model and (f) van't Hoff plot

adsorption is a complex combination of both intraparticle diffusion and surface adsorption.

Thermodynamics of Adsorption

The temperature has an influential effect on the adsorption process. The temperature effect was observed at temperatures 298 K, 313 K, 323 K, and 333 K. It was observed that the percent adsorption increases with an increase in temperature, indicating the chemisorption nature as a minimum amount of activation energy is required for the reaction to proceed. The values of Gibbs free energy (ΔG), enthalpy (ΔH), and entropy (ΔS) were obtained from intercept and slope of plot ln K *versus* 1/T. The negative value of ΔG over the entire temperature range shows the process is spontaneous and exothermic. The positive values of ΔH and ΔS show that the process is entropy driven. The respective van't Hoff plots are shown in Fig. 9f and the results are summarized in Table 2.

Comparison of Adsorption Capacity

Table 3 shows adsorption capacities of various materials reported for the adsorption of various reactive dyes. The table is self-explanatory and shows a comparative account of adsorption capacity with natural materials reported in the literature.

Table 1 — Isotherm and kinetic parameters

S. No.	Models	Parameter	Values
		Adsorption Isotherm	
1	Langmuir	q_m (mg/g)	40.12
		b (L/mg)	0.0399
		R_L	0.3334
		R^2	0.9931
2	Freundlich	K_F ($mg^{1-1/n}$/g/L)	3.4955
		n	0.799
		R^2	0.986
		Adsorption Kinetics	
1	Pseudo-first order	K_1	0.0243
		R^2	0.998
2	Pseudo-second order	K_2	0.0012
		R^2	0.997
3	Intraparticle diffusion	K_{int}	1.982
		R^2	0.974

Table 2 — Thermodynamic parameters

Temperature (K)	ΔG (kJ mol^{-1})	ΔH (kJ mol^{-1})	ΔS (J K^{-1} mol^{-1})
298	–2.422	120.4	413.03
313	–9.547	–	–
318	–10.957	–	–
323	–12.546	–	–

Table 3 — Comparison with the reported literature

Material	Adsorption capacity (mg g^{-1})		Lit. Ref.
Ethylene diamine modified rice husk	16	(R16)	[42]
Organofunctionalized kenyaite	33	(R16)	[43]
Humin immobilized on silica	19.45	(R16)	[44]
Surfactant zeolites	12.6	(R16)	[45]
Aluminium Residue	6.88	(RR133)	[46]
Pinus sylvestris linneo	19.69	(R195)	[47]
Pinus sylvestris linneo	6.72	(RY145)	[48]
CCA	40.12		This work

Conclusions

A CCA composite was successfully synthesized and characterized using various techniques. The data obtained from the characterizations confirmed the formation of a composite. SEM micrographs and EDAX techniques showed surface modifications as well as its composition. BET surface area measurement, performed using the nitrogen adsorption–desorption method, revealed a microporous nature of the adsorbent. CCA was employed to remove R-21 dye from an aqueous medium, along with carbon capture. The amount of dye adsorption was dependent on the adsorbent dosage, temperature, and contact time. The maximum quantity adsorbed on CCA, obtained using the Langmuir model was 40.12 mg g^{-1}. The thermodynamic data suggested that the adsorption of R-21 dye on CCA was spontaneous and endothermic in nature and was entropy-driven. The adsorption mechanism of the R-21 dye on CCA surface could be assigned to various types of interactions, such as electrostatic attraction or H-bonding interaction. The adsorption results indicated that CCA can be a promising alternative for the cleansing of aqueous environments from anionic dyes. Sustainability parameter evaluation has added a new dimension to the studies.

Author Contributions

PN — methodology, investigation, data analysis, validation, writing first draft; RJ — conceptualization, writing: review and editing, supervision.

Funding

This research received no external funding.

Data Availability Statement

Data will be made available on request.

Conflict of interest

The authors declare that there are no conflict of interest for this manuscript.

Acknowledgement

The authors are grateful to RTM Nagpur University for instrumentation and laboratory facilities. Thanks are also due to DST, New Delhi for DST-FIST grant and UGC for UGC-SAP support.

References

1 Kahu S, Shekhawat A, Saravanan D & Jugade R. *Int J Env Sci Tech*, 13 (2016) 2269.
2 Diana S Orietta L Alexandra M Marta F. *Starch* 73 (2021) 2000043.
3 Rakhshaee R Panahandeh M. *J. Hazard. Mater.* 189 (2011) 158.
4 Samoila P, Enache A C, Maria I, Cojocaru C & Harabagiu V, Chitin and Chitosan: Properties and Applications (Wiley: Hoboken, NJ, USA) 2019.
5 Das M & Adholeya A, *Water Chall Solut Glob Scale*, 1206 (2015) 319.
6 Makhado E, Motshabi B, Allouss D, Ramohlola K, Modibane K, Hato M, Jugade R, Shaik F & Pandey S, *Chemosphere,* 306 (2022) 35524.

7 Jiang X, Li Y & Tang X, *Env Sci Poll Res*, 28 (2021) 46934.
8 Udayakumar G, Muthusamy S, Selvaganesh B, Sivarajasekar N, Rambabu K, Sivamani S, Sivakumar N, Maran J & Bandegharaei A, *Biotechnol Adv*, 52 (2021) 107815.
9 Abdelhamid H & Mathew A, *Front Chem Eng*, 3 (2021) 790314.
10 No H & Meyers S, *Rev Env Cont Toxicol*, 163 (2000) 1.
11 Bustos-Terrones Y, Bandala E, Moeller-Chávez G & Bustos-Terrones V, *Water Sci Eng*, 15 (2022) 125.
12 Pandey S & Kang M, *Korean Soc Ind Chem*, 1 (2019) 155.
13 Saruchi M, Kumar V, Ghfar A & Pandey S, *Polymers*, 14 (2022) 1911.
14 Ahmed M, Hameed B & Hummadi E, *Carbohydr Poly*, 247 (2020) 116690.
15 Rodrigues D, Moura J, Dotto G, Cadaval T & Pinto L, *J Poly Env*, 26 (2018) 2917.
16 Wang Y, Wang H, Peng H, Wang Z, Wu J & Liu Z, *Fibers Poly,* 19 (2018) 340.
17 Yildirim A, *Chem Eng Tech,* 44 (2021) 1371.
18 García-González A, Zavala-Arce R, Avila-Pérez P, Rangel-Vazquez N, Salazar-Rábago J, García-Rivas J & García-Gaitán B, *Int J Biol Macromol*, 169 (2021) 75.
19 Usman M, Ahmed A, Yu B, Wang S, Shen Y & Cong H, *Carbohy Poly*, 255 (2021) 117486.
20 Eltaweil A, Hashem O, Abdel-Hamid H, El-Monaem E & Ayoup M, *Int J Biol Macromol*, 222 (2022) 1465.
21 Ilyas R A, Aisyah H A, Nordin A H, Ngadi N, Zuhri M Y M, Asyraf M R M, Sapuan S M, Zainudin E S, Sharma S & Abral H, *Polymers*, 14 (2022) 874.
22 Khapre M, Pandey S & Jugade R, *Int J Biol Macromol*, 190 (2021) 862.
23 Khapre M & Jugade R, *Chem Afr*, 4 (2021) 993.
24 Khapre M & Jugade R, *Water Sci Technol,* 82 (2020) 715.
25 Korde S, Deshmukh S, Tandekar S & Jugade R, *Carb Poly Tech Appl*, 2 (2021) 100081.
26 Khapre M, Shekhawat A, Saravanan D, Pandey S & Jugade R, *Mat Adv*, 3 (2022) 3278.
27 Nandanwar P M, Saravanan D, Bakshe P & Jugade R M, *Mat Adv*, 3 (2022) 5488.
28 Nandanwar P, Jugade R, Gomase V, Shekhawat A, Bambal A, Saravanan D & Pandey S, *J Comp Sci*, 7(2023) 103.
29 Tandekar S, Saravanan D, Korde S & Jugade R, *Mat Today Pro,* 29 (2020) 726.
30 Radjai H, Ferkous Z, Jebali H, Majdoub R, Bourzami G & Raffin M, *Achour A Gil M J Mol Liq*, 361 (2022) 119670.
31 Jeyaseelan C, Chaudhary N & Jugade R, *Air Soil Water Res,* 11 (2018) 1178622118811680.
32 Agu A, Benablo P, Mesias V & Penaloza D, *J Chil Chem Soc,* 64 (2019) 4610.
33 Gomase V, Jugade R, Doondani P, Saravanan D & Pandey S, *Inorg Chem Comm,* 145 (2022) 110009.
34 Chen M, Runge T, Wang L, Li R, Feng J, Shu X & Shi Q, *Carbohy Poly*, 200 (2018) 115.
35 Sing K & Williams R, *Adsorp Sci Tech,* 22 (2004) 773.
36 Korde S, Tandekar S & Jugade R, *J Env Chem Eng*, 8 (2020) 104360.
37 Doondani P, Jugade R, Gomase V, Shekhawat A, Bambal A & Pandey S, *Water*, 14 (2022) 3411.
38 Freundlich H, *J Phys Chem,* 57 (1906) 385.
39 Langmuir I, *J Am Chem Soc,* 40 (1918) 1361.
40 Weber W & Morris J, *J Sanit Eng Div Am Soc Civil Eng*, 89 (1963) 3.
41 Egor M, Kumar A, Ahuja T, Mukherjee S, Chakraborty A, Sudhakar C, Srikrishnarka P, Bose S, Ravindran S & Pradeep T, *ACS Sustain Chem Eng*, 9 (2021) 12788.
42 Lee C K, Ong S T & Zainal Z, *Int J Env Poll,* 34 (2008) 246.
43 Royer B, Cardoso N, Lima E, Ruiz V, Macedo T & Airoldi C, *J Colloid Inter Sci*, 336 (2009) 398.
44 Jesus A M D, Romão L P C, Araújo B R, Costa A S & Marques J J, *Desalination*, 274 (2011) 13.
45 Fungaro D A, Borrely S I & Carvalho T E, *Am J Env Prot,* 1 (2013) 1.
46 Silva T C, Fraga T J M, Carvalho M, Silva V L & Da Motta M A, *Latin Am App Res*, 48 (2018) 101.
47 Aksakal O & Ucun H, *J Haz Mat*, 181 (2010) 666.